Available online at www.sciencedirect.com
ScienceDirect
Journal of Power Sources 179 (2008) 793–798
JOURNAL OF POWER SOURCES
www.elsevier.com/locate/jpowsour

Short communication

Capacity fade analysis of a lithium ion cell

Qi Zhang, Ralph E. White *

Department of Chemical Engineering, University of South Carolina, Columbia, SC 29208, USA

Received 3 December 2007; received in revised form 7 January 2008; accepted 8 January 2008
Available online 21 January 2008

Abstract

A physics-based single particle model was used to simulate the life cycling data of a lithium ion cell. The simulation indicates that there are probably three stages of capacity fade in a lithium ion cell used at low rates. In the first stage, lithium ions are lost to a film formation reaction (e.g. SEI formation) and, consequently, the cathode becomes less intercalated during cycling. In the second stage, the loss of active cathode material outpaces the loss of lithium ions and the cathode gradually becomes more intercalated at the end of discharge. The anode is the limiting electrode in stages one and two and the change in the anode voltage causes the cell to reach end of discharge voltage. In the third stage, the limiting electrode shifts from the anode to the cathode, and the anode becomes increasingly less discharged at the end of discharge. Thus, more and more "cyclable" lithium ions are left inside the anode, which causes additional capacity fade.

Keywords: Life prediction; Limiting electrode

1. Introduction

Secondary lithium ion batteries are being actively researched for the application into aerospace, medical, military and transportation applications. Battery life prediction is an important and active research area. A substantial amount of work [1–11] has gone into understanding the capacity fade and predicting battery life. For example, Stamps et al. [6] studied the capacity fade of a lithium ion cell over 1600 cycles using a hybrid estimation algorithm combining elements of both batch estimation and online moving horizon estimation. However, the battery model used in their work was a simplified empirical model which does not provide insight concerning capacity fade mechanisms. Gang et al. [7] used a physics based model to simulate the cycling performance of lithium ion cells. The SEI formation on the anode during charge was assumed to account for the capacity fade. Lee et al. [8] simulated the cycling performance of lithium ion cells under low earth orbit conditions using the same model. Good agreement was achieved between the experimental and simulated discharge capacities. Other researchers [11] also used equivalent circuit models (ECM) to study the capacity fade of lithium ion cells.

In order to understand how the capacity fade in individual electrodes would affect the capacity fade at the cell level, we used a physics-based single particle model [9,10] to analyze the cycling data of a lithium ion cell. In comparison, most empirical methods such as experimental data extrapolation view the cell as a whole entity and could not provide us such information.

The focus of this work is to show a significant findings based on our data analysis on the cycling data of a lithium ion cell, but not to develop a new cell model. Our study reveals the capacity fade of the cell could have three stages under low rate. The experimental data show the first two stages, controlled mostly by loss of active lithium ions and loss of active cathode material, respectively. A third stage with accelerating capacity fade, as predicted by our simulation, would happen when the limiting electrode shifts from the anode to the cathode. The detailed discussion on this capacity fade sequence can be found in Section 3 of this paper. Although our experimental data have not yet confirmed this three stage capacity fade pattern, Bloom et al. [4] observed a similar pattern in their cycle life study (Fig. 3 in Ref. [4]). However, without further detailed analysis, it is not suggested that our findings can be applied directly to their study.

To our best knowledge, there has not been any publication (in terms of simulation) in the literature to show a similar three-stage capacity fade pattern as ours. We also provide a detailed and plausible explanation on the reasons behind the formation of the three-stage pattern. In addition, our findings highlight

* Corresponding author. Tel.: +1 803 777 3270; fax: +1 803 777 6769.
E-mail addresses: White@engr.sc.edu, REW@SC.EDU (R.E. White).

0378-7753/$ – see front matter © 2008 Elsevier B.V. All rights reserved.
doi:10.1016/j.jpowsour.2008.01.028

Nomenclature

c_e	Li^+ concentration in the electrolyte (mol cm^{-3})
c_{max}	maximum Li^+ concentration in the particles (mol cm^{-3})
c_s	Li^+ concentration in the solid particles (mol cm^{-3})
$\bar{c}_s$	volume averaged Li^+ concentration inside spherical particles (mol cm^{-3})
D_s	solid phase Li^+ diffusion coefficient in the particles (cm^2 s^{-1})
I_{app}	applied current (A)
j_{int}	intercalation current density (A cm^{-2})
k	kinetic rate constant
n	number of terms in Eq. (5)
R_s	radius of the spherical particles (cm)
U	open circuit potential of the electrode (V)
V	volume of the electrode (cm^3)
x	the stoichiometric number at the discharged state
x_0	the stoichiometric number at the charged state

Greek letters

ε	volume fraction of the active material in the electrode
λ_m	positive eigen-value determined from $\lambda_m = \tan(\lambda_m)$.
Φ	electrode potential (V)

Subscripts

i	positive or negative electrode
neg	negative electrode
pos	positive electrode

the importance to consider the interaction between individual electrodes and the cell in making the cycle life predictions. We believe these contributions could provide useful information for battery researchers to consider in their own studies.

2. Model

The experimental discharge capacities are presented in Fig. 1 for a lithium ion cell (1Ah) with a $LiNiCoO_2$ cathode and a carbon anode. The discharge current was 8 mA (<C/100). The discharge data were studied using a so-called single particle model [9,10]. The model uses the assumption that the behavior of the porous electrodes can be represented by spherical particles of the active materials in the electrodes. The concentration and potential distributions in the solution phase are assumed to be negligible, which is a reasonable assumption under low rate situations. Therefore, the usage of the single particle model is limited to low current situations. The detailed description and discussion of the single particle model can be found in the literature [9,10].

The model equations consist of the solid phase diffusion equation (Fick's diffusion law) in a spherical particle and the

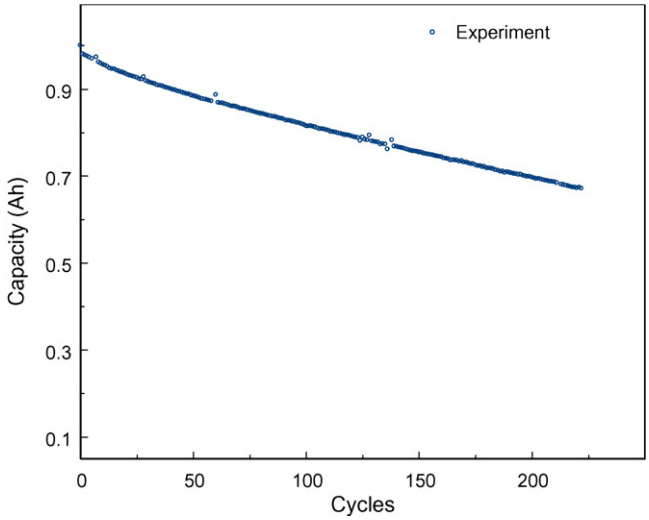

Fig. 1. The experimental discharge capacities vs. cycles.

Butler Volmer equation for both electrodes:

$$\frac{\partial c_{s,i}}{\partial t} = \frac{1}{r^2}\frac{\partial}{\partial r}\left(D_{s,i} r^2 \frac{\partial c_{s,i}}{\partial r}\right), \quad -D_{s,i}\left.\frac{\partial c_{s,i}}{\partial r}\right|_{r=0} = 0,$$
$$-D_{s,i}\left.\frac{\partial c_{s,i}}{\partial r}\right|_{r=R_{s,i}} = \frac{j_{int,i}}{F} \tag{1}$$

$$j_{int,i} = k_i c_e^{0.5}(c_{max,i} - c_{s,i}|_{r=R_{s,i}})^{0.5}\, c_{s,i}|_{r=R_{s,i}}{}^{0.5} \times \left[\exp\left(\frac{0.5F}{RT}(\Phi_i - U_i)\right) - \exp\left(\frac{-0.5F}{RT}(\Phi_i - U_i)\right)\right] \tag{2}$$

The intercalation current density $j_{int,i}$ is calculated based on the equivalent electro-active surface area (A_i) of the electrode "i":

$$j_{int,i} = \frac{I_{app}}{A_i} = \frac{I_{app}}{3/R_{s,i}\varepsilon_i V_i} \tag{3}$$

where V_i is the volume of the electrode and ε_i is the volume fraction of the active electrode material. The decrease of the volume fraction ε_i could indicate a loss of active material in the electrode (i.e., through isolation of active material particles from the electrode).

The diffusion equation (Eq. (1)) can be further simplified from a partial differential equation to a differential and algebraic equation using the pseudo steady state (PSS) method [12,13]. The PSS equations for the diffusion in the electrode "i" are:

$$\frac{\partial \bar{c}_{s,i}}{\partial t} = -\frac{3}{R_{s,i}}\frac{j_{int,i}}{F} \tag{4}$$

$$(c_{s,i}|_{r=R_{s,i}} - \bar{c}_{s,i}) = -\frac{j_{int,i}}{F}\frac{R_{s,i}}{5D_{s,i}} + \frac{2R_{s,i}}{D_{s,i}}\frac{j_{int,i}}{F} \times \sum_{m=1}^{n} \frac{\sqrt{1+\lambda_m^2}}{\lambda_m^2}(-1)^m \sin(\lambda_m)\, e^{-\lambda_m^2 D_{s,i} t/R_{s,i}^2} \tag{5}$$

where the number of terms "n" in the summation is typically set equal to 5; $\bar{c}_{s,i}$ the volume averaged concentration in the spherical particle, and $c_{s,i}|_{r=R_{s,i}}$ is the concentration at the surface of the particle. The state of charge (SOC) or the stoichiometric number of the electrode is defined as

$$x_i = \frac{\bar{c}_{s,i}}{c_{\max,i}} \tag{6}$$

The λ_m values are determined from the eigen-value equation:

$$\lambda_m = \tan(\lambda_m) \tag{7}$$

3. Results and discussion

3.1. Parameter estimation

Three model parameters were found to change with cell capacity fade when fitting the discharge data. They are the initial SOCs for the cathode and the anode at the beginning of charge ($x_{0,pos}$ and $x_{0,neg}$), and the volume fraction of the cathode (ε_{pos}). The volume fraction of the anode does not change much with cycling. Fig. 2 compares the experimental and simulated discharge curves at selected cycles and the model parameters are listed in Table 1.

Fig. 3 shows the change of the three model parameters with cycling. The anode and the cathode become consistently less charged with cycling ($x_{0,pos}$ increases and $x_{0,neg}$ decreases). It is more severe for the anode than for the cathode. The volume fraction of the cathode ε_{pos} decreases, indicating that the cathode loses active material with cycling.

Fig. 4 shows the predicted values of SOCs for the anode (x_{neg}) and the cathode (x_{pos}) at the end of discharge (EOD) for each cycle. A two-stage pattern is clearly seen in Fig. 4 for the electrode SOCs. The cathode becomes less intercalated at EOD in the first stage, then more intercalated in the second stage. Although the anode SOC changes in a similar pattern, it must be

Table 1
Model parameters used in the study

Parameters	Anode	Cathode
Maximum solid phase concentration (mol cm^{-3}), $c_{\max,i}$	3.056E−2	5.156E−2
Solid phase diffusion coefficient (cm^2 s^{-1}), $D_{s,i}$	1E−11	2E−10
Rate constant (cm$^{2.5}$ mol$^{-0.5}$ s^{-1}), k_i	1.07E−4	6.36E−5
Molecular weight (g mol^{-1}), MW$_i$	72	97.68
Particle size (cm), $R_{s,i}$	5E−4	5E−4
Electrode volume (cm^3), V_i	4.1	3.5
Initial SOC of the electrode, $x_{0,i}$[a]	0.823	0.2925
Volume fraction of active material, ε_i[b]	0.3749	0.34
Electrolyte concentration (mol cm^{-3}), c_e	1.0E−3	

[a] Initial SOCs for the anode and the cathode would change during cycling. The value for the first cycle is shown in the table.
[b] The volume fraction of active material for the cathode decreases with cycling. The value is shown for the first cycle.

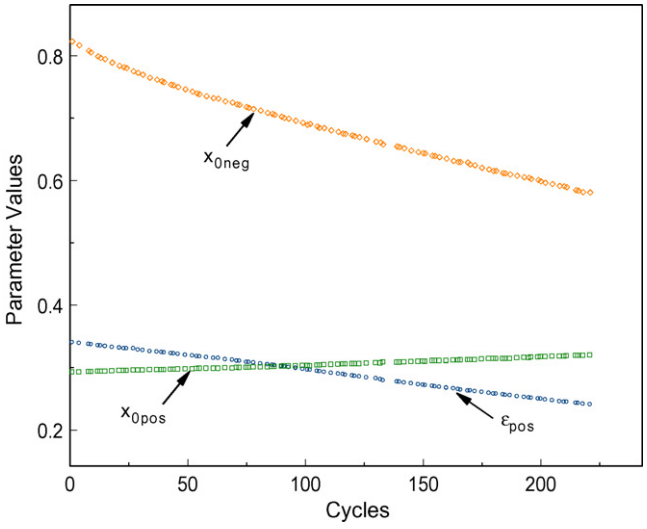

Fig. 3. The change of model parameters with cycles (obtained from fitting the discharge data for each cycle). Both the anode and the cathode become less charged, as $x_{0,neg}$ decreases and $x_{0,pos}$ increases. The volume fraction of the cathode ε_{pos} decreases, indicating that the cathode loses some active material with cycling.

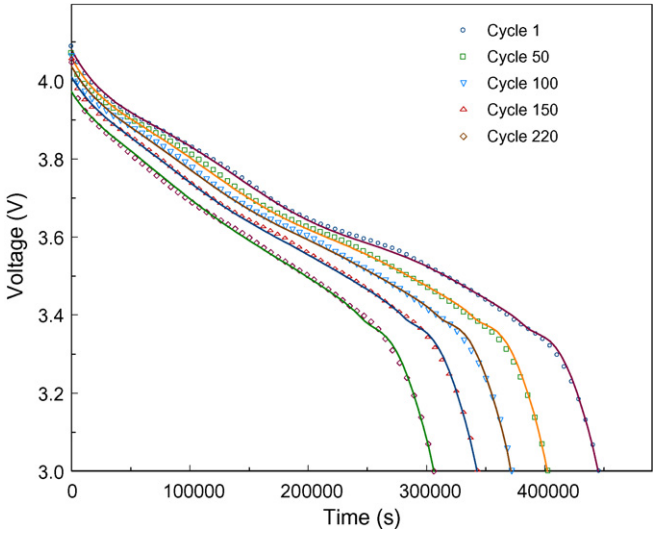

Fig. 2. Comparison of the experimental and simulated discharge curves at selected cycles. The symbols are experiment data and the lines are the simulation predictions. The discharge current was 1 mA.

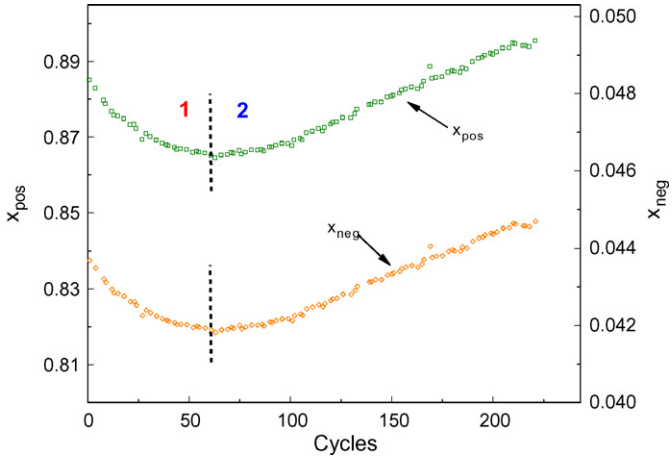

Fig. 4. The simulated SOCs for the anode and the cathode at the end of discharge (EOD) predicted by the model using parameters shown in Fig. 3. A two-stage behavior is clearly seen from the figure for the electrode SOCs.

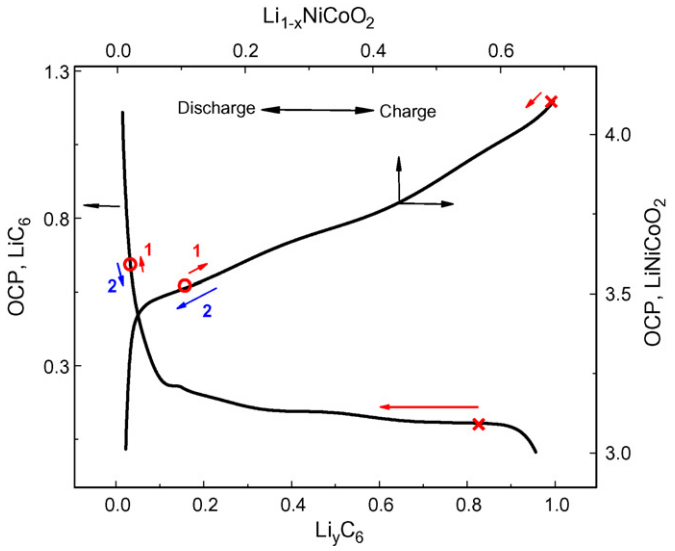

Fig. 5. The change of stoichiometric windows (or SOCs) for the electrodes with cycling. The cross marker (✕) indicates the movement for $x_{0,pos}$ and $x_{0,neg}$ and the circle marker (○) indicates the movements for x_{pos} and x_{neg} (SOC at the EOD). Note the cathode OCP is plotted against $1-x$ in $Li_{1-x}NiCoO_2$. Both electrodes become less charged with cycling. A two-stage pattern is observed for the electrode SOC at the EOD (refer to Fig. 4 for x_{pos} and x_{neg}).

noted that the anode SOC at EOD changes on a much smaller scale, between 0.042 and 0.045, as compared to the cathode SOC at EOD. A detailed discussion on the two-stage pattern is presented below. Movements of the stoichiometric windows for the electrodes are summarized in Fig. 5.

3.2. Model prediction

The model parameters are extrapolated in Fig. 6 (see Table 2). The assumption is that the capacity fade mechanisms remain unchanged during the period of our prediction.

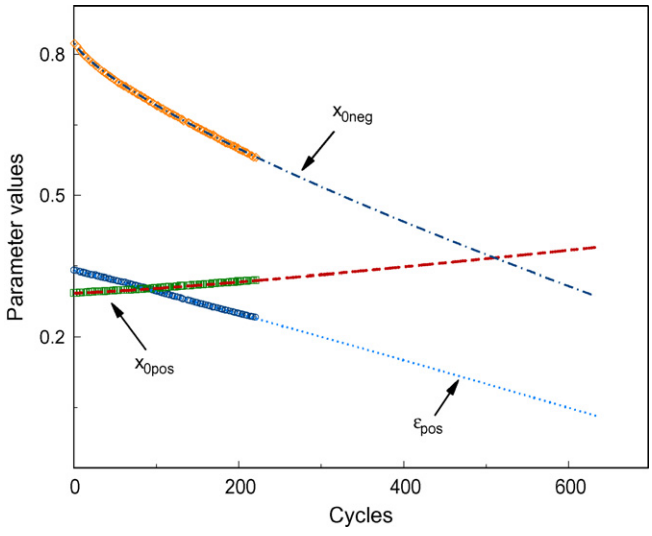

Fig. 6. The extrapolation of the model parameters shown in Fig. 3. The expressions used for the extrapolation are listed in Table 2.

Table 2
The extrapolation expressions for the parameters shown in Fig. 6

Parameters	Expression	a	b	c
$x_{0,pos}$	ax^b+c	3.656E−5	1.221	0.2928
$x_{0,neg}$	ax^b+c	−4.262E−3	0.7507	0.8267
ε_{pos}	ax^b+c	−3.468E−4	1.053	0.3406

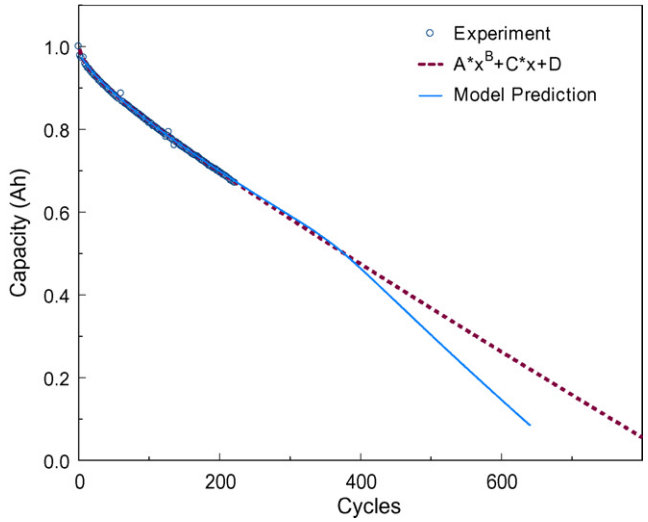

Fig. 7. The discharge capacities predicted by the model compared to the one predicted by the empirical expression. A stage of accelerated capacity fade is predicted by the physics-based model.

The predicted discharge capacity as a function of cycle number is shown in Fig. 7 using the extrapolated model parameters. A stage of accelerating capacity fade is predicted after about 390 cycles. Also shown in Fig. 7 is a prediction of the discharge capacities obtained by using an empirical equation (see Table 3). It should be mentioned that researchers [4] have observed capacity fade patterns shaped in a similar means to that shown in Fig. 7.

Fig. 8 shows the simulated electrode SOCs at the EOD using the extrapolated model parameters. Please note that the scale for x_{neg} in Fig. 8 is different from the one used in Fig. 4. A third stage is observed for the change of x_{pos} and x_{neg} with cycling. The SOC of the cathode at the EOD becomes mostly fixed at 0.98 in this stage, indicating that the cathode is close to being fully intercalated. The SOC of the anode, however, increases dramatically (less discharged) at the EOD, as compared to the negligible movement in the first two stages. Fig. 9 shows the movement of the SOCs for the electrodes in all the three stages.

By comparing Figs. 6 and 7, it is found that the appearance of the three stages for the electrode SOCs at the EOD

Table 3
Parameter values for the empirical expression used in Fig. 7

Expression	Ax^B+Cx+D
A	−0.00971
B	0.5007
C	-8.03×10^{-3}
D	0.9946

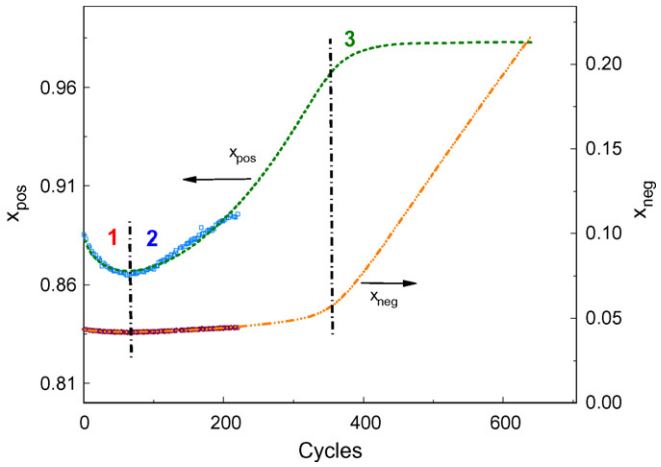

Fig. 8. The simulated SOCs for the anode and the cathode at the EOD using extrapolated model parameters shown in Fig. 6. The symbols represent the SOC data plotted in Fig. 4. Please note the scale for x_{neg} is different from the one in Fig. 4. A third stage shown for x_{pos} and x_{neg} is predicted by the model.

corresponds to the different capacity fade stages shown in our discharge capacity predictions. Next, we will analyze the capacity fade of the cell based on the information obtained using the physics-based model.

3.3. Capacity fade analysis

Our study shows that there could be multiple stages in the capacity fade of the cell. In this section, the scenarios behind those stages for cell capacity fade are presented.

The parameter estimation study shows that the volume fraction of the cathode decreases with cycling (ε_{pos} in Fig. 3), indicating that the cathode loses some of the active material in the electrode. In addition, it is well known that there are side reactions happening on the anode during charge process, which would consume the cyclable lithium ions to form SEI

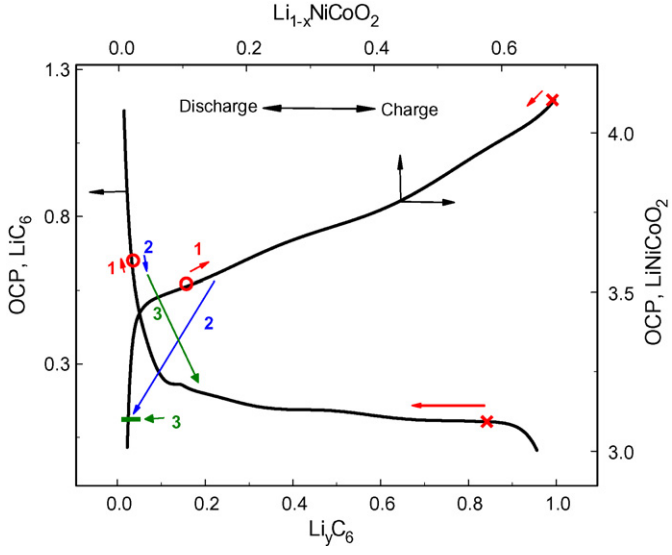

Fig. 9. The simulated SOCs for the electrodes at the EOD using extrapolated model parameters.

film on the anode. The major capacity fade mechanisms in the cell simulated here are expected to be the loss of lithium ions to a film formation reaction and the loss of active material in the cathode.

The loss of lithium ions to a film formation reaction controls the capacity fade in the first stage, because the film formation reaction rate is relatively high on a fresh cell. It is estimated that during the first charge/discharge cycle, about 18% of the charge capacity is irreversibly lost to the film formation [14]. In our case, the cathode is charged from $Li_{(1.0)}NiCoO_2$ to $Li_{(0.3)}NiCoO_2$ ($x_{0,pos} \approx 0.3$ in Fig. 3) on the first charge. Then the cathode is only intercalated back to $Li_{(0.89)}NiCoO_2$ at the end of first discharge ($x_{pos} \approx 0.89$ in Fig. 4). The loss ratio is (1–0.89)/(1–0.3) = 0.16. That is, 16% of the charge capacity (1–0.3) is irreversibly lost to the film formation for the first cycle, which is in good agreement with the 18% estimation in Ref. [14]. After the first cycle, the side reaction rate gradually decays, because the SEI film on the anode partially impedes the further occurrence of the side reaction. This is supported by the observation that the capacity fade rate decreases initially, and the decrease of $x_{0,neg}$ slows with cycling.

In the first stage of capacity fade, the anode is the limiting electrode. Here the limiting electrode refers to the one which is fully discharged at the EOD and causes the cell to reach end of discharge voltage. The circle marker (O) in Fig. 9 shows clearly that the anode is fully discharged at EOD. The cathode, on the other hand, is not fully intercalated, because some lithium ions have been irreversibly consumed by the film formation reaction. As the loss of lithium ions becomes larger, the cathode is continuously less intercalated at the EOD, leading to a decreasing x_{pos} as shown in Fig. 8.

In the second stage, the controlling capacity fade mechanism shifts from the loss of lithium ions to the loss of active cathode material. As mentioned previously, the film formation reaction rate decays in the first stage after the SEI film forms on the anode, leading to a slower loss of lithium ions. The loss of active cathode material then gradually outpaces the loss of lithium ions, which causes the cathode to become more intercalated at the EOD (x_{pos} increases in Fig. 8). Fig. 8 shows this transition point as a minimum in the x_{pos} versus cycles, where the loss of cathode material starts to outpace the loss of lithium ions. However, the anode is still the limiting electrode in the second stage. Fig. 8 shows that the anode is mostly discharged to the SOC below 0.05 in the second stage, which can be regarded as fully discharged at the EOD. Although the SOC of the cathode (x_{pos}) at the EOD increases with the cycling, it is not the cathode that causes the cell to reach the EODV in the second stage.

In the third stage, the capacity fade mechanisms remain the same as in previous stages. However, the limiting electrode has been shifted from the anode to the cathode. Fig. 8 shows that the cathode is nearly fully discharged (to $Li_{1.0}NiCoO_2$) at the beginning of the third stage. The anode becomes increasingly less discharged at the EOD. More and more "cyclable" lithium ions are left inside the anode and cannot be intercalated back into the cathode. The holding capacity of the cathode decreases further as the cathode loses more active material. In return, more

"cyclable" lithium ions are kept inside the anode at the EOD, causing accelerating capacity fade.

4. Conclusions

A physics-based single particle model is used to study the cycling data of a lithium ion cell. Parameter estimation technique is applied to extract model parameters from the experiment discharge data. The study on the experiment data shows that there are two stages in the cell capacity fade. Model simulation further indicates that there is a third stage of capacity fade yet to come where the limiting electrode shifts from the anode to the cathode.

The loss of lithium ions to a film formation reaction (SEI formation) and the loss of active cathode material are the major capacity fade mechanisms. In the first stage, the loss of lithium ions to the film formation reaction is the controlling mechanism. However, the side reaction rate decays after the SEI film forms on the anode. The cathode becomes less intercalated at the EOD as cyclable lithium ions are irreversibly consumed in the film formation reaction. The anode is the limiting electrode in the first stage. In the second stage, the loss of active cathode material outpaces the loss of lithium ions because of the decay of the film formation reaction rate. The cathode becomes more intercalated at the EOD. The anode is still the limiting electrode. In the third stage, the limiting electrode shifts from the anode to the cathode. Because the anode could not be fully discharged, "cyclable" lithium ions are left inside the anode, causing the accelerating capacity fade.

Acknowledgement

We are grateful for the financial support of the project by the National Reconnaissance Office (NRO) under contract # NRO-000-03-C-0122.

References

[1] R.B. Wright, C.G. Motloch, J.R. Belt, J.P. Christophersen, C.D. Ho, R.A. Richardson, I. Bloom, S.A. Jones, V.S. Battaglia, G.L. Henriksen, T. Unkelhaeuser, D. Ingersoll, H.L. Case, S.A. Rogers, R.A. Sutula, J. Power Sources 110 (2002) 445.
[2] P. Nelson, I. Bloom, K. Amine, G. Henriksen, J. Power Sources 110 (2002) 437.
[3] I. Bloom, S.A. Jones, V.S. Battaglia, G.L. Henriksen, J.P. Christophersen, R.B. Wright, C.D. Ho, J.R. Belt, C.G. Motloch, J. Power Sources 124 (2003) 538.
[4] I. Bloom, B.G. Potter, C.S. Johnson, K.L. Gering, J.P. Christophersen, J. Power Sources 155 (2006) 415.
[5] Q. Zhang, R.E. White, J. Power Sources 173 (2007) 990.
[6] A.T. Stamps, C.E. Holland, R.E. White, E.P. Gatzke, J. Power Sources 150 (2005) 229.
[7] N. Gang, R.E. White, B.N. Popov, Electrochim. Acta 51 (2006) 2012.
[8] J.W. Lee, Y.K. Anguchamy, B.N. Popov, J. Power Sources 162 (2006) 1395.
[9] G. Ning, B.N. Popov, J. Electrochem. Soc. 151 (2004) A1584.
[10] S. Santhanagopalan, Q. Guo, P. Ramadass, R.E. White, J. Power Sources 156 (2006) 620.
[11] B.Y. Liaw, R.G. Jungst, G. Nagasubramanian, H.L. Case, D.H. Doughty, J. Power Sources 140 (2005) 157.
[12] Q. Zhang, R.E. White, J. Power Sources 165 (2007) 880.
[13] S. Liu, Solid State Ionics 177 (2006) 53.
[14] V. Srinivasan, J. Newman, J. Electrochem. Soc. 151 (2004) A1530.